Size-Dependent Optical Properties of InP Colloidal Quantum Dots

Guilherme Almeida,[1] Lara van der Poll,[1] Wiel H. Evers,[1] Emma Szoboszlai,[1] Sander Vonk,[2] Freddy T. Rabouw[2] and Arjan J. Houtepen[1]*

[1]Optoelectronic Materials Section, Faculty of Applied Sciences, Delft University of Technology, Van der Maasweg 9, 2629 HZ Delft, The Netherlands.

[2]Debye Institute for Nanomaterials Science, Utrecht University, Princetonplein 1, 3584 CC, Utrecht, The Netherlands

KEYWORDS InP, quantum dots, phosphors, absorption, luminescence

ABSTRACT: Indium phosphide colloidal quantum dots (CQDs) are the main alternative for toxic and restricted Cd based CQDs for lighting and display applications. Here we systematically report on the size-dependent optical absorption, ensemble and single particle photoluminescence (PL) and biexciton lifetimes of core-only InP CQDs. This systematic study is enabled by improvements in the synthesis of InP CQDs to yield a broad size series of monodisperse core-only InP CQDs with narrow absorption and PL linewidth and significant PL quantum yield.

Introduction. InP colloidal quantum dots (CQDs) have raised considerable interest for photonic technologies operating in the visible and near-infrared, because of their tunable band gap in the range of 1.3 ~ 3 eV, strong light absorption, efficient luminescence and compliance with European safety regulations on electronic products (ROHS).[1] However, the size dependent optical properties of InP CQDs have not been reported to the level of detail that is common for other CQDs. This is due to difficulties in synthesizing luminescent samples of various sizes with narrow size distributions free of dopants (e.g. Zn) or shells (e.g. $ZnSe_{1-x}S_x$). In this regard, considerable progress has been recently achieved. On one hand the works of Won et al., Li et al. and Xu et al. laid down synthetic procedures to obtain monodisperse InP CQDs over a wide size-range.[2-4] On the other hand, recent work by some of the authors have shown that highly luminescent InP CQDs can be obtained by simply passivating their surface with In-based Z-type ligands, provided that the CQDs are oxide-free.[5]

By combining these methods, we prepare a size series of nearly mono-disperse and bright InP CQDs with band gaps spanning a considerable portion of the visible spectrum and determine several fundamental size dependent optical properties. First we determine and quantify their sizing curves and light absorption characteristics by employing a combination of structural techniques and atomistic models. Radiative rates are extracted from photo-luminescence (PL) transients recorded using time-correlated single-photon counting, and single dot PL linewidths are measured by single-dot spectroscopy. Finally, power-dependent charge carrier recombination is investigated using transient absorption spectroscopy which allows to extract biexciton lifetimes and Auger constants.

Results and discussion. A size series of InP CQDs is prepared following reported procedures but conducting the syntheses under a hydrogen containing argon atmosphere of high purity in order to mitigate oxidation.[6] While bulk InP has a band gap of ca. 1.33 eV, the InP CQDs studied in this work exhibit first-absorption-peak-energies (E_{1s}) in the range of 2.0 to 2.7 eV (620 to 460 nm), and thus cover a considerable portion of the visible spectrum. The narrow size-distributions of these samples can be appreciated from the well-defined features in their absorbance spectra, shown in Figure 1a. The full-width-at-half-maximum (FWHM) of the 1S exciton absorption peak decreases from 273 meV to 146 meV with increasing QD size.

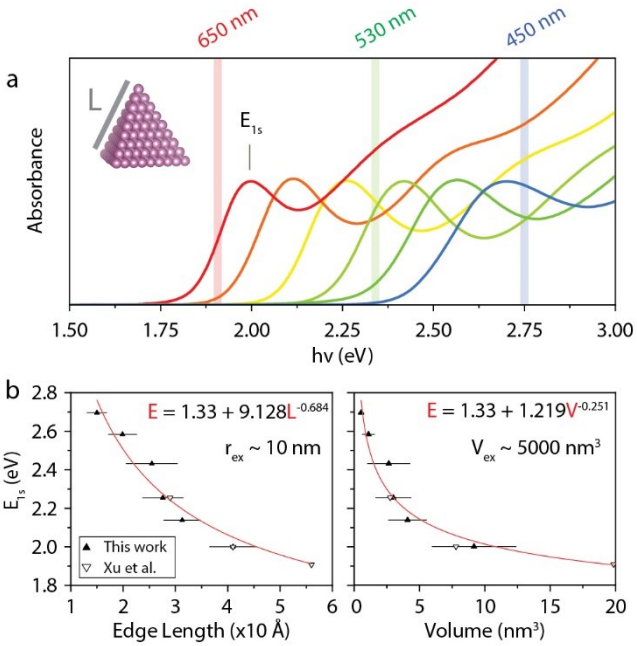

Figure 1- (a) The absorbance spectra of InP CQDs investigated in this work exhibit well-defined features characteristic of nearly mono-disperse samples. Morphological analysis reveals that the QDs adopt a pyramidal shape and allows to build (b) sizing curves relating the energy of the first-absorption-peak (E_{1s}) with the average edge length and geometrical volume. It can be seen that these QDs are much smaller than the InP exciton Bohr radius (r_{ex}) or volume (V_{exc}): they are therefore in the strong quantum confinement regime

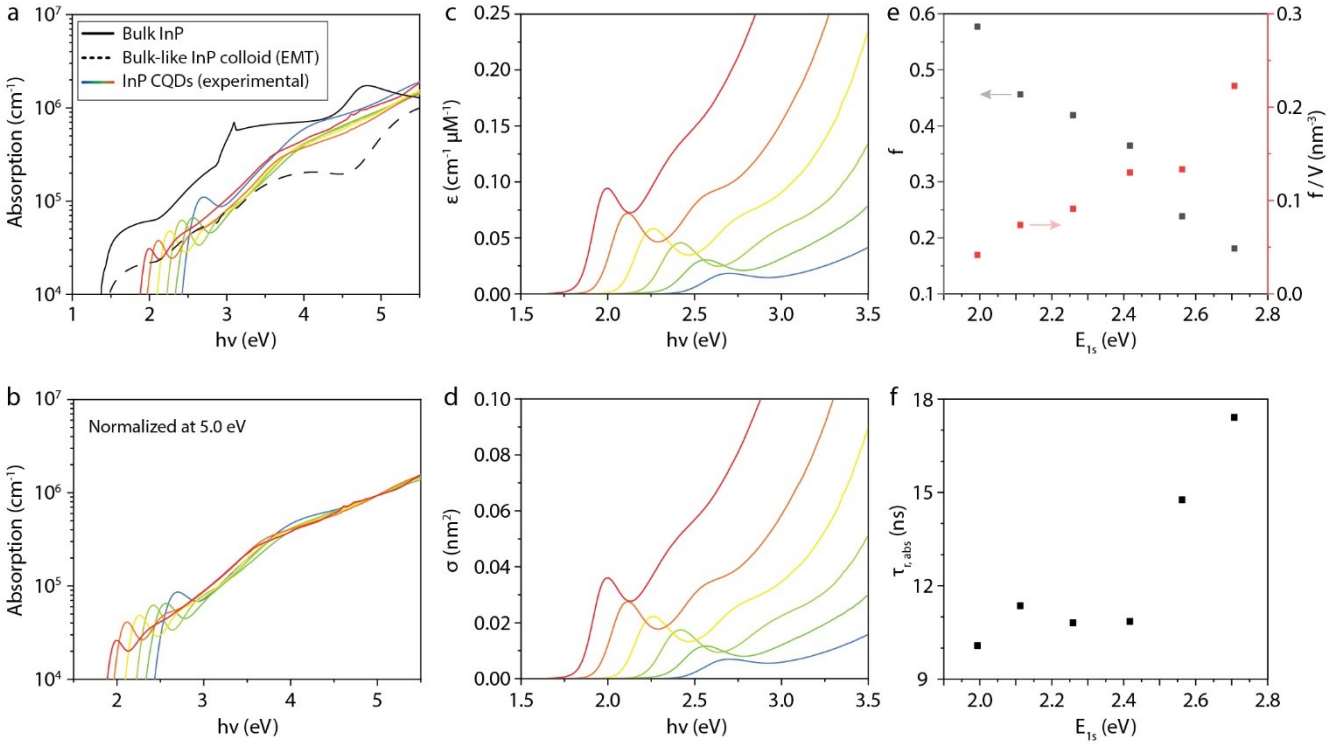

Figure 2- Absorptive properties of InP CQDs.(a) The experimental (intrinsic) absorption coefficient α_i of InP CQDs (in heptane) is plotted alongside that of bulk InP and that of an hypothetical bulk-like InP colloid (calculated following the Effective Medium Theory model). Assuming that the absorption coefficients of the QDs converge at energies well above the gap, we (b) normalize the spectra to an average value at 5.0 eV. The (c) extinction coefficients and the (d) cross sections are subsequently determined from the normalized α_i spectra. Finally, the (e) oscillator strength and the (f) lifetime of the band edge transitions are derived from the cross sections.

InP QDs with band gaps in the visible range are relatively small when compared with other visible emitting QDs such as CdSe for instance, as shown in Figure S1 of the Supporting Information (SI).[7] This is not surprising since bulk InP has charge-carrier effective masses that are similar to those of CdSe but a band gap that is 400 meV narrower. The smallest QDs in our series have an edge length of 1.5 nm (corresponding to 5 In atoms), and a E_{1s} of 2.70 eV (460 nm). The smaller the QDs the tighter the size distributions necessary for narrow ensemble linewidths. On top of that, QD single particle linewidths also appear to broaden with decreasing size,[8-10] and this is also the case for InP QDs as shown below. This partially explain the difficulties in obtaining InP CQDs with narrow emission linewidths in the visible and makes the absorption spectra with distinct features particularly noteworthy.

We start by relating E_{1s} with the number-weighted average size and volume, determined from the analysis of electron micrographs shown in Figure S2. InP CQDs appear to adopt a (regular) tetrahedral shape, in line with previous reports,[4, 11] which allows their geometrical volume $V_{QD}=L^3/(6\sqrt{2})$ to be determined analytically from their edge length L. Our InP CQDs exhibit edge lengths (volumes) in the range of 1 to 4 nm (1-10 nm^3). They are much smaller than the exciton Bohr radius (volume) which is ca. 10 nm (5000 nm^3),[12] and are therefore in the strong quantum confinement regime. The sizing curves are reported in Figure 1b. We have included extra data points from the work of Xu et al. for comparison and to extend the curves on the red side.[4] It is found that $E_{1s} \approx 1.33+1.219\ V_{QD}^{-0.251}$, with E_{1s} in eV and V_{QD} in nm^3.

We also determine the energy of the second transition by taking the second derivative of the absorbance spectra and identifying the second negative peak. As shown in Figure S3, the energy of this transition and its separation from E_{1s} is also size-dependent.

Next, we quantify the absorption strength of InP QDs as a function of size, an important property for e.g. phosphor applications. The (intrinsic) absorption coefficient α_i is first estimated experimentally through the Lambert-Beer law[13]

$$A = \varepsilon\,[QD]\,l = \frac{\alpha_i\, V_{QD}\, N_A}{\ln(10)}\,[QD]\,l$$

where A is the absorbance, ε is the extinction coefficient, l is the path length, and N_A is Avogadro's number. The concentration of QDs, denoted [QD], is estimated as described in the SI. Briefly, it is estimated from the concentration of In atoms, measured via ICP-OES, assuming that the QDs are fully In-terminated and hence have a size-dependent stoichiometry (extracted from atomistic models). In addition, we consider volumes based on the discrete number of atoms, i.e. $V_{QD}=V_{In}N_{In}+V_PN_P$ (the atomic radius of Phosphorus (207pm) is obtained from the InP unit cell, while that of Indium (109pm) is obtained from tabulated values.[14] These atom-based volumes are slightly larger than geometrical volumes but more accurate, as they fully account for surface atoms. Geometrical volumes do not account for surface atoms in full and introduce an important size dependent error, as shown in Figure S2f, due to the size-dependent fraction of surface atoms in QDs (see also note 1 in the SI).

The experimental estimates of α_i (in heptane) are plotted in Figure 2a, alongside the bulk absorption coefficient α_b. First, we note that α_i of InP CQDs is considerably smaller than α_b due to the dielectric screening of the electromagnetic field that occurs for small colloids in solution. These effects can be taken into account using effective medium approaches like the Maxwell-

Garnett model.[13] Therefore we also calculate the absorption coefficient of a bulk-like InP colloid α_{bc}, which, according to this model, is defined as

$$\alpha_{bc} = \frac{n_b \alpha_b}{n_s} |f_{LF}|^2$$

where n_b is the real part of the refractive index of bulk InP, n_s is the refractive index of the solvent (constant, 1.39 for heptane) and f_{LF} is is the local field factor, which in turn is defined as

$$f_{LF} = \frac{3\varepsilon_s}{\varepsilon_b + 2\varepsilon_s}$$

for spherical colloids, where ε_b is the complex dielectric function of bulk InP and ε_s that of the solvent ($\varepsilon_s = n_s^2$ for a transparent solvent such as heptane). Note that no analytical expression is available for tetrahedrons, but the effect of shape is likely small.

The estimated values of α_i of InP CQDs appear to be in the same order of magnitude as α_{bc} except for the 3.5-5 eV region. On one hand, we note that α_{bc} should only be taken as a rough guide as the optical constants of the QDs must differ from that of bulk and the InP QDs are not spherical. On the other hand, the deviation could also arise from the absorption of (metal)organic species or even InP clusters that might be present in the samples.[4, 15]

Our estimates for α_i of InP CQDs follow the trend that is usually observed, i.e. they are strongly size dependent at the band edge but seem to converge at energies well above the gap.[13] We assume that, at high energies, the minor deviation in α_i between samples is due to experimental uncertainties. Therefore we rescale the α_i spectra such that the new value at 5.0 eV equals the average value in the six measurements (Figure 2b).

The extinction coefficient ($\varepsilon = \alpha_i V_{QD} N_A / \ln(10)$) and the absorption cross section ($\sigma = \alpha_i V_{QD}$) are subsequently determined from the normalized α_i spectra and shown in Figures 2c and 2d, respectively. At E_{1s}, the extinction coefficient of InP QDs appears to be roughly half that of their equivolumetric CdSe counterparts, but at high energies (ca. 4 eV) it appears to be higher,[7, 16] similar to what is observed in bulk or for bulk-like colloids (see Figure S1).

The oscillator strength *f* of the band edge transitions is determined from the cross sections using the expression[17-18]

$$f = \frac{4m\varepsilon_0 c}{e^2} \int_{\nu 1}^{\nu 2} \sigma \, d\nu$$

where ν1 and ν2 are the start and end frequencies of the band edge transition, *m* is the mass and *e* is the charge of an electron, ε_0 is the permittivity of free space and c is the speed of light. The cross sections were fit with Gaussian curves to extract the contribution of the band edge transition (see Figure S4). The oscillator strength of the band edge transition is found to decrease with decreasing QD size (black data points in Figure 2e), however, when *f* is normalized by the QD volume, the opposite trend can be observed (red data points in Figure 2e), in line with the size dependence of α_i at the band edge (see Figure 2a).

Finally, the expected radiative lifetime ($\tau_{r,abs} = 1/A_i$) of the band edge transition can also be derived from the cross section through the Einstein coefficient (A_i) defined as[17-18]

$$A_i = \frac{8\pi}{\lambda^2} \int_{\nu 1}^{\nu 2} \sigma \, d\nu$$

where λ is the wavelength of the optical transition. The computed radiative lifetimes of the band edge transition are plotted in Figure 2f: they are in the 10-20 ns range and increase with decreasing QD size. These computed radiative lifetimes will be compared to measured PL lifetimes below.

We note that given its complexity, there is a significant error associated with the quantification of the absorptive properties. Such errors are however too difficult to determine given the many sources of error involved (weighing, dilutions, elemental quantification, size distributions, surface composition etc.). We tried to minimize errors as much as possible and the data presented herein are in line with expectations.

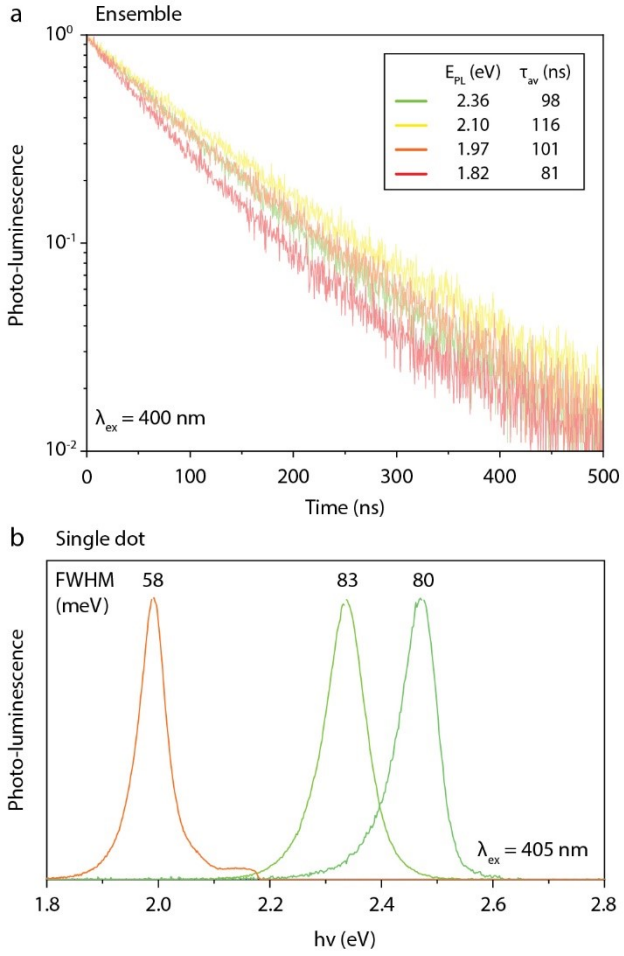

Figure 3– Luminescent properties of InP QDs. (a) PL decays of ensembles are recorded using time-correlated single-photon counting and are fit with bi-exponential decays with an amplitude average lifetime τ_{av}. Photo-luminescence quantum yields (Φ_{PL}) are in the range of 50 to 80%. (b) Single-dot PL spectra exhibit full widths at half maximum (FWHM) of ca. 60 and 80 meV in the red and in the green, respectively.

Photo-luminescence (PL) transient of CQD ensembles are recorded using time-correlated single-photon counting and shown in figure 3a. These PL transients are not single exponential but are well described by a bi-exponential function (fits are shown in Figure S6 and summarized in Table S1). The lifetimes of the

main component (τ_1) are in the range of 60-90 ns while the weaker component exhibits lifetimes that are roughly twice longer ($\tau_2 \approx$ 150-200 ns). This yields amplitude-weighted average lifetimes (τ_{av}) in the range of 80-120 ns.[19-20]

Importantly, the expected radiative lifetimes calculated earlier from the absorption cross sections ($\tau_{r,\,abs}$, shown in Figure 2b) are 6 times shorter than τ_1 and ca. 5-8 times shorter than τ_{av}. This discrepancy can be explained by the fine structure of the band edge exciton.[21-22] Briefly, in most semiconductors the ground exciton state is a dark state and in small sized II-VI and III-V CQDs strong spatial confinement yields considerable splitting between the fine structure levels. The absorption is dominated by transitions to a bright exciton level with the highest oscillator strength. After excitation, relaxation brings the exited state to a thermal population over the lowest energy dark state and a bright state about several meV above it. The oscillator strength of this emissive bright state is lower than that of the absorbing bright state, and it is only partially populated at room temperature, which explains why the observed PL lifetime is longer than that calculated from the absorption coefficient. Similar conclusions have been drawn for InP/$ZnSe_{1-x}S_x$ core/shell CQDs.[23-25] The results presented here suggest a similar fine structure for core-only InP QDs.

We also note that the PL lifetimes of red-emitting quasi type-I InP/$ZnSe_{1-x}S_x$ core/shell QDs with near unity quantum yields are considerably shorter, about 30 ns.[2, 26] However, it is unknown to what extent core-only and core-shell CQDs differ in fine structure,[27] In addition InP/$ZnSe_{1-x}S_x$ core/shell QDs have a different electron-hole overlap, with the electron wavefunction delocalizing into the shell, and hence also higher oscillator strengths given their much larger volumes. The fact that our InP core-only CQDs do not reach unity quantum yields also adds uncertainty to the analysis of the PL transients. On one hand, the PL transients most likely describe a sum of different transients from particles of varying QY.[28] On the other hand, we cannot rule out that delayed luminescence may also contribute to the observed long PL lifetimes.

Next, single-dot PL spectra are measured using PL microscopy. First we note that these InP QDs exhibit blinking (Figure S8). Their PL spectra, shown in Figure 4b, exhibit full widths at half maximum of ca. 60 and 80 meV in the red and in the green, respectively, which is considerably narrower than ensemble PL spectra (> 200 meV in our samples). Both the values and the size-dependent trend are in good agreement with what is normally observed from single dots of other compositions.[8-10] The single-dot spectrum is determined by the combined effect of phonon coupling and emission from multiple fine-structure states.[8] In addition, we find, that one of our single-QD measurements showed spectral diffusion of approximately 50 meV on timescale of seconds (see Figure S8), which suggests that spectral diffusion might contribute significantly to line broadening.

The relatively narrow single-QD linewidths of 60–80 meV and much broader ensemble linewidths (200 meV) are consistent with previous studies on InP-based core/shell QDs.[29] Recent work has confirmed that InP-based core/shell QDs can have narrow single-QDs linewidths, but also showed that they on average suffer more from spectral diffusion (Figure S8b) and that inhomogeneous broadening is more significant than for CdSe-based QDs.[30] Our measurements in Figure 3b show narrow single-QD linewidths even for core-only InP QDs. This is encouraging, as it promises the possibility of narrower linewidths in InP CQDs with improved surface passivation or engineered electron-phonon coupling.[8-10]

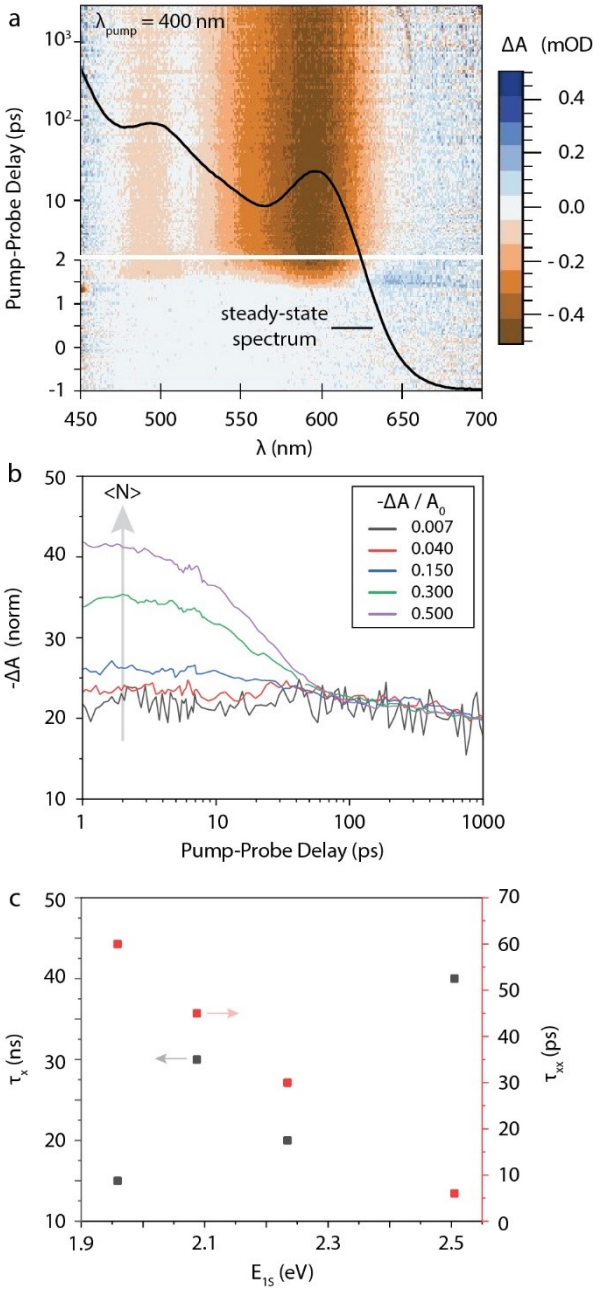

Figure 4 - Transient absorption (TA) spectroscopy of InP CQDs. A typical TA spectrum is shown in panel (a). The kinetic analysis of (b) the band edge bleach at various pump powers (here defined by maximum value of $-\Delta A/A_0$) allows to extract (c) the single-exciton (τ_x) and the bi-exciton lifetimes (τ_{xx}), and subsequently, to derive the Auger Constant for bi-excitons (shown in SI).

Finally, the kinetics of photo-generated charge carriers are investigated using power-dependent transient-absorption (TA) spectroscopy. A typical lower power TA map, showing the change in absorption as a function of time and wavelength in false colors, is shown in Figure 4a (see Figure S9 for all TA

maps). Briefly, exciting the samples at energies above the bandgap quickly(<1ps) leads to a bleach of the band edge (1S) transition. The decay of the band edge bleach is then analyzed as a function of pump-power (see Figures 4b, S10 and S11). At low powers, the large majority of excited QDs only has one exciton and the decays can be fit to a single-exponential decay with lifetime τ_x shown in Figure 4c. It can be seen that these single-exciton decays are in the order of 10-40 ns and appear to increase with QD size, however, since the maximum delay time of the measurement is 3 ns, these lifetimes are out of the measurement range and have a large associated uncertainty.

As the pump power is increased, so does the fraction of excited QDs with two or more excitons. This leads to the appearance a fast component in the 10-100 ps-timescale, as can be seen in Figure 3b, which is assigned to the fast Auger recombination. At intermediate powers the decays can be described by adding a second exponential decay with lifetime τ_{xx}, shown in Figure 4c. These bi-exciton lifetimes are quite short, in the range of 5 to 60 ps and correspond to Auger Constants ($AC=V^2(8\ \tau_{xx})^{-1}$)[31] in the range of 0.05 to 1 ($x10^{30}$) $cm^6\ s^{-1}$ (see Figure S12). The values are in line with previous measurements on $InP/ZnSe_{1-x}S_x$ core shell QDs[2] as well as with the universal size-dependent trend of Auger constants proposed by Robel et al.[32]. This shows that the scaling of Auger recombination in these small InP core-only QDs is similar to that of other QD materials.

Conclusion. Using recently developed protocols we have synthesized a size series of monodisperse and highly luminescent InP core-only QDs. This series enables, for the first time, the systematic study of the size dependent optical properties of core only InP QDs.

Based on absorption measurements we report the size dependence of the bandgap, second optical transition, absorption coefficient, oscillator strength and associated radiative lifetime of the 1S absorption transition. Time resolved PL measurements yield PL lifetimes significantly longer than that expected from the absorption strength, showing that PL involves a different fine-structure level than the absorption. Single particle PL measurements reveal narrow single particle linewidths of 60-80 meV at room temperature. Transient absorption measurement allow to determine the size dependent biexciton lifetime, which follows previously reported volume scaling trends for other QD materials.

Overall, the observed trends of the absorption coefficient, oscillator strength and biexcton lifetime agree quite well with those obtained on other QD materials, after taking into account the bulk optical properties of InP and the generally smaller size of visible emitting InP CQDs when compared to CdSe CQDs.

ASSOCIATED CONTENT

Supporting Information (SI).

AUTHOR INFORMATION

Corresponding Author

* A.J.Houtepen@tudelft.nl

Present Addresses

Author Contributions

GA and AH conceived the study. GA and WE designed and built the synthetic apparatus. GA and LP prepared the samples. GA and ES performed the structural modeling and EMT calculations. GA performed all optical characterization except luminescence microscopy which was performed by SV. WE performed the TEM imaging. GA analyzed the data and wrote the manuscript with guidance and input from SV, FR and AH.

Funding Sources

This publication is part of the project Quantum Dots for Advanced Lightning Applications (QUALITy)) with Project No. 17188 of the Open Technology Programme which is (partly) financed by the Dutch Research Council (NWO).

ACKNOWLEDGMENT

The authors thank collaborators at the TU Delft, namely, Michel van den Brink for the ICP analyses, Zimu Wei and Jos Thieme for their assistance with TA measurements, and Deepika Poonia for her help with the cross-section fittings.

Graphical TOC

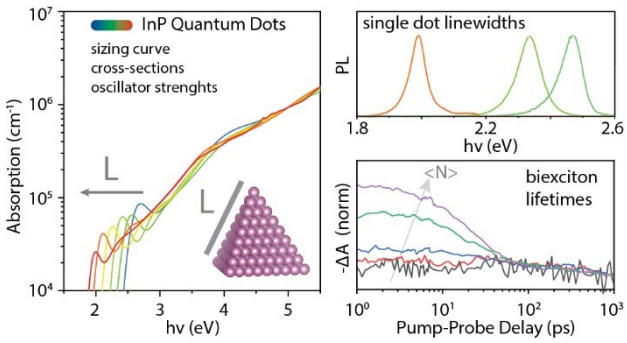

Methods

All synthetic procedures are executed in air-free conditions (Schlenk line or glovebox, $H_2O < 0.1$ ppm, $O_2 < 0.1$ ppm).

Materials. Palmitic acid (PA, 99%), myristic acid (99%), palmitic acid (99%), trioctylphosphine (TOP, 97%), heptane (99%, anhydrous) and acetone (99.8%, anhydrous) are purchased from Merck Sigma and used as received. Tris(trimethylsilyl)phosphine (98%, Strem), indium(III) fluoride (99.95%, anhydrous, Alfa Aesar), In(III) acetate (99.99%, anhydrous, Thermo Scientific), hexadecane (99%, anhydrous Thermo Scientific) are used as received. Octadecene (ODE, 90%, Merck Sigma) is degassed *in vacuo* at 100°C before being stored in a glovebox. Aqua regia is prepared using ultra-pure nitric and hydrochloric acids (Optima grade, Thermo Fisher). Argon (6N) and Argon (6N) mixed with 2% vol. Hydrogen (6N) are purchased from Linde.

Synthesis of InP CQDs. The smallest dots are synthesized following the procedure of Xu et al., intermediate ones through the method of Wu et al. and the largest ones according to that of Li et al.. Importantly, all the QDs are prepared under an ultra-pure argon – hydrogen atmosphere. At the end of the synthesis, the QDs are transferred inside an air-free glovebox, washed with acetone (three times) and re-dispersed in heptane.

In(III) Palmitate (0.2M) is prepared by heating a mixture of In(III) acetate, palmitic acid (3 eq.) and 1-octadecene in two stages. First under vacuum (<0.1 mbar) up to 100 °C and then at 150 °C under vigorous Ar (6N) bubbling for 30 minutes. The solution is then stored inside an air-free glovebox. We note that In-palmitate precipitates out of solution at room-temperature, and is therefore homogenized by heating (to ca. 100 °C) before use.

Surface Passivation with InX_3 is conducted according to previous reported protocols inside an air-free glovebox.[5] Briefly, InP CQDs (0.5 mL, 40 μM in dry hexadecane or 1-octadecene) are combined with InF_3 (50 mg, 0.29 mmol) and In(III) palmitate (100 μL of a 0.2 M solution) inside a glass vial (the amounts are indicative and were in fact adjusted slightly depending on the size of the QDs). The vial is tightly capped and the mixture is stirred at 150 °C for one hour. After cooling, InF_3 is separated out by centrifugation and the bright CQDs are washed with acetone and re-dispersed in heptane.

Transmission Electron Microscopy. Samples are drop cast onto grids and imaged on a JEOL JEM3200FSC microscope. The data is obtained using zero loss imaging (20eV) in counting mode and is movie corrected by SerialEM with a Gatan K2 summit camera.

Inductively Coupled Plasma Optical Emission Spectroscopy. Dry QD samples are digested in aqua regia (ca. 0.5 mL) inside a plastic tube), diluted with a HNO_3 solution (ca. 10 mL, 0.5 M, in ultra-pure milli-Q water) to achieve a concentration of In in the range of 1 ppm and analyzed using a Spectro Arcos spectrometer (detection range: 10 ppb to 20 ppm). The concentrations are determined against an external calibration.

Steady-State Absorption and Luminescence Spectroscopies. UV-Vis absorbance spectra are recorded on a Perkin-Elmer Lambda 365 spectrometer. Fluorescence measurements are recorded on an Edinburgh Instruments FLS980 spectrometer equipped with PMT detectors. For fluorescence measurements, the samples are loaded into air-tight cuvettes. Photo-luminescence quantum yields are measured in accordance with IUPAC methodology,[33] against a coumarin 102 dye solution in ethanol at an excitation wavelength of 387 nm. Measuring the coumarin 102 quantum yield in an integrating sphere in the same setup gave a value of 99%, but to calculate the quantum yield, the literature value of 95% is considered for the quantum yield of coumarin 102. [34]

Time-Correlated Single Photon Counting (TCSPC). Samples are loaded into air-tight cuvettes and photo-luminescence decays are collected on an Edinburgh Instruments Lifespec setup equipped a 400 nm pulsed laser. Amplitude-weighted lifetimes are calculated by the following equation: $\tau_{av}=(A_1\tau_1+A_2\tau_2)/(A_1+A_2)$ where A_n and τ_n are the n-th amplitude and lifetime parameters obtained from the bi-exponential fit.[19-20]

fs-Transient Absorption (TA) Spectroscopy . QD dispersions are loaded into air-tight cuvettes for TA measurements which are then conducted on a Light Conversion TA Setup. Briefly, an IR pulse (1028 nm, 180 fs) is producted by a Yb-KGW oscillator (Light Conversion, Pharos SP) at a frequency of 5 kHz. The pulse is split in two, one part is converted into a pump beam (wavelength tunable) by an optical parametric amplifier , while the other part is used to produce a broadband probe by supercontinuum generation in a sapphire crystal. Pump and probe beams overlap at the sample position with a small angle, with a relative time delay controlled by an automated delay-stage and the probe is then directed onto a photo-detector (Ultrafast Systems, Helios). During the experiments, we make sure the pump and probe beams have orthogonal polarizations (i.e. one of them is vertically polarized, the other horizontally), to reduce the influence of pump scattering into our detector. The pump beam is transmitted through a mechanical chopper operating at 2.5 kHz, allowing one in every two pump pulses to be transmitted. This allows to obtain pump-on and pump-off spectra, from which the differential absorbance $\Delta A = \log(I_{on}/I_{off})$ is determined (I is the probe light incident on the detector with either pump on or pump off). TA data are corrected for probe-chirp via a polynomial correction to the coherent artifact. Photon fluences are estimated by measuring the (pump) power with a thermopile sensor (Coherent, PS19Q) and taking into account the overlap of the pump and probe beams (imaged with a beamprofiler).

Photo-Luminescence Microscopy measurements are performed on a home-built optical setup consisting of a Nikon Ti-U inverted microscope body. A 405-nm diode laser (Picoquant D-C 405, controlled by Picoquant PDL 800-D laser driver) was guided to the sample by a dichroic mirror (edge at 425 nm, Thorlabs DMLP425R) and an oil-immersion objective (Nikon CFI Plan Apochromat Lambda 100x, NA 1.45). The QD emission was collected by the same objective and guided to a spectrometer (Andor Kymera 193i, 150 lines/mm reflective grating) with an electron-multiplying CCD detector (Andor iXon Ultra 888). To minimize photobleaching due to oxidation reactions, we deposit the nanocrystals on a glass coverslip inside a nitrogen-purged glovebox. We subsequently seal the QDs in between the coverslip and a microscope slide using an airtight spacer to ensure an oxygen-free environment during our measurements.

REFERENCES

1. Almeida, G.; Ubbink, R.; Stam, M.; Houtepen, A., InP Colloidal Quantum Dots for Visible and Near-Infrared Photonics. *Nature Reviews Materials (accepted)* **2023**.
2. Won, Y.-H.; Cho, O.; Kim, T.; Chung, D.-Y.; Kim, T.; Chung, H.; Jang, H.; Lee, J.; Kim, D.; Jang, E., Highly efficient and stable InP/ZnSe/ZnS quantum dot light-emitting diodes. *Nature* **2019,** *575* (7784), 634-638.
3. Li, Y.; Hou, X.; Shen, Y.; Dai, N.; Peng, X., Tuning the Reactivity of Indium Alkanoates by Tertiary Organophosphines for the Synthesis of Indium-Based Quantum Dots. *Chemistry of Materials* **2021,** *33* (23), 9348-9356.
4. Xu, Z.; Li, Y.; Li, J.; Pu, C.; Zhou, J.; Lv, L.; Peng, X., Formation of Size-Tunable and Nearly Monodisperse InP Nanocrystals: Chemical Reactions and Controlled Synthesis. *Chemistry of Materials* **2019,** *31* (14), 5331-5341.
5. Ubbink, R. F.; Almeida, G.; Iziyi, H.; du Fossé, I.; Verkleij, R.; Ganapathy, S.; van Eck, E. R. H.; Houtepen, A. J., A Water-Free In Situ HF Treatment for Ultrabright InP Quantum Dots. *Chemistry of Materials* **2022,** *34*, 10093–10103.
6. Baquero, E. A.; Virieux, H.; Swain, R. A.; Gillet, A.; Cros-Gagneux, A.; Coppel, Y.; Chaudret, B.; Nayral, C.; Delpech, F., Synthesis of Oxide-Free InP Quantum Dots: Surface Control and H2-Assisted Growth. *Chemistry of Materials* **2017,** *29* (22), 9623-9627.
7. Jasieniak, J.; Smith, L.; van Embden, J.; Mulvaney, P.; Califano, M., Re-examination of the Size-Dependent Absorption Properties of CdSe Quantum Dots. *The Journal of Physical Chemistry C* **2009,** *113* (45), 19468-19474.
8. Cui, J.; Beyler, A. P.; Coropceanu, I.; Cleary, L.; Avila, T. R.; Chen, Y.; Cordero, J. M.; Heathcote, S. L.; Harris, D. K.; Chen, O.; Cao, J.; Bawendi, M. G., Evolution of the Single-Nanocrystal Photoluminescence Linewidth with Size and Shell: Implications for Exciton–Phonon Coupling and the Optimization of Spectral Linewidths. *Nano Letters* **2016,** *16* (1), 289-296.
9. Yazdani, N.; Volk, S.; Yarema, O.; Yarema, M.; Wood, V., Size, Ligand, and Defect-Dependent Electron–Phonon Coupling in Chalcogenide and Perovskite Nanocrystals and Its Impact on Luminescence Line Widths. *ACS Photonics* **2020,** *7* (5), 1088-1095.
10. Kang, S.; Kim, Y.; Jang, E.; Kang, Y.; Han, S., Fundamental limit of emission linewidth of quantum dots: ab initio study on CdSe nanocrystals. *ACS Applied Materials & Interfaces* **2020,** *12*, 22012–22018.
11. Kim, K.; Yoo, D.; Choi, H.; Tamang, S.; Ko, J.-H.; Kim, S.; Kim, Y.-H.; Jeong, S., Halide–Amine Co-Passivated Indium Phosphide Colloidal Quantum Dots in Tetrahedral Shape. **2016,** *55* (11), 3714-3718.
12. Korti-Baghdadli, N. M., Abdelkrim Elhasnaïne Benouaz, Tayeb, Adjusted Adashi's Model of Exciton Bohr Parameter and New Proposed Models for Optical Properties of III-V Semiconductors. *American Journal of Materials Science and Technology* **2013,** *3*, 65-73.
13. Hens, Z.; Moreels, I., Light absorption by colloidal semiconductor quantum dots. *Journal of Materials Chemistry* **2012,** *22* (21), 10406-10415.
14. Shannon, R., Revised effective ionic radii and systematic studies of interatomic distances in halides and chalcogenides. *Acta Crystallographica Section A* **1976,** *32* (5), 751-767.
15. Gary, D. C.; Terban, M. W.; Billinge, S. J. L.; Cossairt, B. M., Two-Step Nucleation and Growth of InP Quantum Dots via Magic-Sized Cluster Intermediates. *Chemistry of Materials* **2015,** *27* (4), 1432-1441.
16. Karel Čapek, R.; Moreels, I.; Lambert, K.; De Muynck, D.; Zhao, Q.; Van Tomme, A.; Vanhaecke, F.; Hens, Z., Optical Properties of Zincblende Cadmium Selenide Quantum Dots. *The Journal of Physical Chemistry C* **2010,** *114* (14), 6371-6376.
17. Hilborn, R. C., Einstein coefficients, cross sections, f values, dipole moments, and all that. *American Journal of Physics* **1982,** *50* (11), 982-986.
18. Yu, P.; Beard, M. C.; Ellingson, R. J.; Ferrere, S.; Curtis, C.; Drexler, J.; Luiszer, F.; Nozik, A. J., Absorption Cross-Section and Related Optical Properties of Colloidal InAs Quantum Dots. *The Journal of Physical Chemistry B* **2005,** *109* (15), 7084-7087.
19. Sillen, A.; Engelborghs, Y., The Correct Use of "Average" Fluorescence Parameters. *Photochemistry and Photobiology* **1998,** *67* (5), 475-486.
20. Zatryb, G.; Klak, M. M., On the choice of proper average lifetime formula for an ensemble of emitters showing non-single exponential photoluminescence decay. *Journal of Physics: Condensed Matter* **2020,** *32* (41), 415902.
21. Sercel, P. C.; Efros, A. L., Band-Edge Exciton in CdSe and Other II–VI and III–V Compound Semiconductor Nanocrystals − Revisited. *Nano Letters* **2018,** *18* (7), 4061-4068.
22. Kim, J.; Wong, C. Y.; Scholes, G. D., Exciton Fine Structure and Spin Relaxation in Semiconductor Colloidal Quantum Dots. *Accounts of Chemical Research* **2009,** *42* (8), 1037-1046.
23. Brodu, A.; Ballottin, M. V.; Buhot, J.; van Harten, E. J.; Dupont, D.; La Porta, A.; Prins, P. T.; Tessier, M. D.; Versteegh, M. A. M.; Zwiller, V.; Bals, S.; Hens, Z.; Rabouw, F. T.; Christianen, P. C. M.; de Mello Donega, C.; Vanmaekelbergh, D., Exciton Fine Structure and Lattice Dynamics in InP/ZnSe Core/Shell Quantum Dots. *ACS Photonics* **2018,** *5* (8), 3353-3362.
24. Brodu, A.; Chandrasekaran, V.; Scarpelli, L.; Buhot, J.; Masia, F.; Ballottin, M. V.; Severijnen, M.; Tessier, M. D.; Dupont, D.; Rabouw, F. T.; Christianen, P. C. M.; de Mello Donega, C.; Vanmaekelbergh, D.; Langbein, W.; Hens, Z., Fine Structure of Nearly Isotropic Bright Excitons in InP/ZnSe Colloidal Quantum Dots. *The Journal of Physical Chemistry Letters* **2019,** *10* (18), 5468-5475.
25. Brodu, A.; Tessier, M. D.; Canneson, D.; Dupont, D.; Ballottin, M. V.; Christianen, P. C. M.; de Mello Donega, C.; Hens, Z.; Yakovlev, D. R.; Bayer, M.; Vanmaekelbergh, D.; Biadala, L., Hyperfine Interactions and Slow Spin Dynamics in Quasi-isotropic InP-based Core/Shell Colloidal Nanocrystals. *ACS Nano* **2019,** *13* (9), 10201-10209.
26. Li, Y.; Hou, X.; Dai, X.; Yao, Z.; Lv, L.; Jin, Y.; Peng, X., Stoichiometry-Controlled InP-Based Quantum Dots: Synthesis, Photoluminescence, and Electroluminescence. *Journal of the American Chemical Society* **2019,** *141* (16), 6448-6452.
27. Sousa Velosa, F.; Van Avermaet, H.; Schiettecatte, P.; Mingabudinova, L.; Geiregat, P.; Hens, Z., State Filling and Stimulated Emission by Colloidal InP/ZnSe Core/Shell Quantum Dots. *Advanced Optical Materials* **2022,** *10* (18), 2200328.
28. Rabouw, F. T.; van der Bok, J. C.; Spinicelli, P.; Mahler, B.; Nasilowski, M.; Pedetti, S.; Dubertret, B.; Vanmaekelbergh, D., Temporary Charge Carrier Separation Dominates the Photoluminescence Decay Dynamics of Colloidal CdSe Nanoplatelets. *Nano Letters* **2016,** *16* (3), 2047-2053.
29. Cui, J.; Beyler, A. P.; Marshall, L. F.; Chen, O.; Harris, D. K.; Wanger, D. D.; Brokmann, X.; Bawendi, M. G., Direct probe of spectral inhomogeneity reveals synthetic tunability of single-nanocrystal spectral linewidths. *Nature Chemistry* **2013,** *5* (7), 602-606.
30. Mangnus, M. J. J.; de Wit, J. W.; Vonk, S. J. W.; Geuchies, J. J.; Albrecht, W.; Bals, S.; Houtepen, A. J.; Rabouw, F. T., High-Throughput Characterization of Single-Quantum-Dot Emission Spectra and Spectral Diffusion by Multiparticle Spectroscopy. *ACS Photonics* **2023**.
31. Klimov, V. I.; McGuire, J. A.; Schaller, R. D.; Rupasov, V. I., Scaling of multiexciton lifetimes in semiconductor nanocrystals. *Physical Review B* **2008,** *77* (19), 195324.
32. Robel, I.; Gresback, R.; Kortshagen, U.; Schaller, R. D.; Klimov, V. I., Universal Size-Dependent Trend in Auger Recombination in Direct-Gap and Indirect-Gap Semiconductor Nanocrystals. *Physical Review Letters* **2009,** *102* (17), 177404.
33. Brouwer, A. M., Standards for photoluminescence quantum yield measurements in solution (IUPAC Technical Report). **2011,** *83* (12), 2213-2228.
34. Jones, G.; Jackson, W. R.; Choi, C. Y.; Bergmark, W. R., Solvent effects on emission yield and lifetime for coumarin laser dyes. Requirements for a rotatory decay mechanism. *The Journal of Physical Chemistry* **1985,** *89* (2), 294-300.